

# Analysis of Circular Torsion Bar with Circular Holes Using Null-field Approach

Jeng-Tzong Chen<sup>1</sup>, Wen-Cheng Shen<sup>2</sup>, Po-Yuan Chen<sup>2</sup>

**Abstract:** In this paper, we derive the null-field integral equation for a circular bar weakened by circular cavities with arbitrary radii and positions under torque. To fully capture the circular geometries, separate forms of fundamental solution in the polar coordinate and Fourier series for boundary densities are adopted. The solution is formulated in a manner of a semi-analytical form since error purely attributes to the truncation of Fourier series. Torsion problems are revisited to demonstrate the validity of our method. Torsional rigidities for different number of holes are also discussed.

**keyword:** Torsion, Null-field integral equation, Fourier series, Circular hole, Torsional rigidity.

## 1 Introduction

Boundary value problems always involve several holes or more than one important reference point. It is convenient to be able to expand the solutions in alternative ways, each way referring to different specific coordinate set describing the same solution. According to the idea, we develop a systematic approach including the adaptive observer system and degenerate kernel for fundamental solution in the polar coordinate and employ Fourier series to approximate the boundary data.

In the past, multiply connected problems have been carried out either by conformal mapping or by special techniques. Ling [Ling C. B. (1947)] solved the torsion problem of a circular tube with several holes. Muskhelishvili [Muskhelishvili N. I. (1953)] solved the problem of a circular bar reinforced by an eccentric circular inclusion. Chen and Weng [Chen T.; Weng I. S. (2001)] have introduced conformal mapping with a Laurent series expansion to analyze the Saint-Venant torsion problem. They concerned with a eccentric bar of different ma-

terials with an imperfect interface under torque. Based on the CVBEM (complex variable boundary element method), Shams-Ahmadi and Chou [Shams-Ahmadi M.; Chou S. I. (1997)] have investigated the torsion problem of composite shafts with any number of inclusions of different materials. Recently, Ang and Kang [Ang W. T.; Kang I. (2000)] developed a general formulation for solving the second-order elliptic partial differential equation for a multiply-connected region in a different version of CVBEM. To avoid mesh generation for finite element or boundary element, meshless formulation is a promising direction [Jin B. (2004), Sladek V.; Sladek J.; Tanaka M. (2005), Wordelman C. J.; Aluru N. R.; Ravaoli U. (2000)]. The present formulation can be seen as one kind of meshless methods, since it belongs to boundary collocation methods. Because the conformal mapping is limited to the doubly connected region, an increasing number of researchers have paid more attentions on special solutions. However, the extension to multiple circular holes may encounter difficulty. It is not trivial to develop a systematic method for solving the torsion problems with several holes. Crouch and Mogilevskaya [Crouch S. L.; Mogilevskaya S. G. (2003)] utilized Somigliana's formula and Fourier series for elasticity problems with circular boundaries. Mogilevskaya and Crouch [Mogilevskaya S. G.; Crouch S. L. (2001)] have solved the problem of an infinite plane containing arbitrary number of circular inclusions based on the complex singular integral equation. In their analysis procedure, the unknown tractions are approximated by using the complex Fourier series. However, for calculating an integral over a circular boundary, they didn't express the fundamental solution using the local polar coordinate. By moving the null-field point to the boundary, the boundary integral can be easily determined using series sums in our formulation due to the introduction of degenerate kernels. Mogilevskaya and Crouch [Mogilevskaya S. G.; Crouch S. L. (2001)] have used the Galerkin method to approach boundary density instead of collocation approach. Our approach can be extended to the Galerkin formulation only for the circular and an-

---

<sup>1</sup>Distinguished Professor, Department of Harbor and River Engineering, National Taiwan Ocean University, Keelung, Taiwan. Email: jtchen@mail.ntou.edu.tw

<sup>2</sup>Graduate student, Department of Harbor and River Engineering, National Taiwan Ocean University, Keelung, Taiwan.

nular cases. However, it may encounter difficulty for the eccentric case. Two requirements are needed: degenerate kernel expansion must be available and distinction of interior and exterior expression must be separated. Therefore, the collocation angle of  $\phi$  is not in the range 0 to  $2\pi$  in our adaptive observer system. This is the reason why we can not formulate in terms of Galerkin formulation using orthogonal properties twice. Free of worrying how to choose the collocation points, uniform collocation along the circular boundary yields a well-posed matrix. On the other hand, Bird and Steele [Bird M. D.; Steele C. R. (1991)] have also used separated solution procedure for bending of circular plates with circular holes in a similar way of the Trefftz method and addition theorem. In this paper, the null-field integral equation is utilized to solve the Saint-Venant torsion problem of a circular shaft weakened by circular holes. The mathematical formulation is derived by using degenerate kernels for fundamental solution and Fourier series for boundary density in the null-field integral equation. Then, it reduces to a linear algebraic equation. After determining the unknown Fourier coefficients, series solutions for the warping function and torsional rigidity are obtained. Numerical examples are given to show the validity and efficiency of our formulation.

## 2 Formulation of the problem

What is given in Figure 1 is a circular bar weakened by  $N$  circular holes placed on a concentric ring of radius  $b$ .

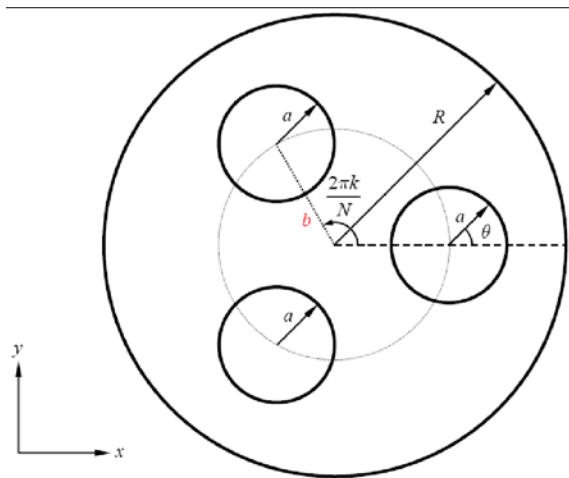


**Figure 1** : Cross section of bar weakened by  $N$  ( $N = 3$ ) equal circular holes

The radii of the outer circle and the inner holes are  $R$  and  $a$ , respectively. The circular bar twisted by couples applied at the ends is taken into consideration. Following the theory of Saint-Venant torsion [Timoshenko S. P.; Goodier J. N. (1970)], we assume the displacement field to be

$$u = -\alpha yz, \quad v = \alpha xz, \quad w = \alpha\varphi(x, y), \quad (1)$$

where  $\alpha$  is the angle of twist per unit length along the  $z$  direction and  $\varphi$  is the warping function. According to the displacement field in Eq. (1), the strain components are

$$\epsilon_x = \epsilon_y = \epsilon_z = \gamma_{xy} = 0, \quad (2)$$

$$\gamma_{xz} = \frac{\partial w}{\partial x} + \frac{\partial u}{\partial z} = \alpha\left(\frac{\partial\varphi}{\partial x} - y\right), \quad (3a)$$

$$\gamma_{yz} = \frac{\partial w}{\partial y} + \frac{\partial v}{\partial z} = \alpha\left(\frac{\partial\varphi}{\partial y} + x\right), \quad (3b)$$

and their corresponding components of stress are

$$\sigma_x = \sigma_y = \sigma_z = \sigma_{xy} = 0, \quad (4)$$

$$\sigma_{xz} = \mu\alpha\left(\frac{\partial\varphi}{\partial x} - y\right), \quad \sigma_{yz} = \mu\alpha\left(\frac{\partial\varphi}{\partial y} + x\right), \quad (5)$$

where  $\mu$  is the shear modulus. There is no distortion in the planes of cross sections since  $\epsilon_x = \epsilon_y = \epsilon_z = \gamma_{xy} = 0$ . We have the state of pure shear at each point defined by the stress components  $\sigma_{xz}$  and  $\sigma_{yz}$ . The warping function  $\varphi$  must satisfy the equilibrium equation

$$\frac{\partial^2\varphi}{\partial x^2} + \frac{\partial^2\varphi}{\partial y^2} = 0 \quad \text{in } D, \quad (6)$$

where the body force is neglected and  $D$  is the domain. Since there are no external forces on the cylindrical surface, we have  $t_x = t_y = t_z = 0$ . By substituting the normal vector, the only zero  $t_z$  becomes

$$t_z = \sigma_{xz}n_x + \sigma_{yz}n_y = 0 \quad \text{on } B. \quad (7)$$

By substituting (5) into (7) and rearranging, the boundary condition is

$$\frac{\partial\varphi}{\partial x}n_x + \frac{\partial\varphi}{\partial y}n_y = yn_x - xn_y = \nabla\varphi \cdot \mathbf{n} = \frac{\partial\varphi}{\partial n} \quad \text{on } B, \quad (8)$$

where  $B$  is the boundary. In Figure 1, we introduce the expressions for the position vector  $(x_k, y_k)$  of the boundary point on the  $k$ th circular hole

$$\begin{aligned} x_k &= a \cos \theta_k + b \cos\left(\frac{2\pi k}{N}\right), \quad k = 1, 2, \dots, N, \\ 0 &< \theta_k < 2\pi, \end{aligned} \quad (9)$$

$$\begin{aligned} y_k &= a \sin \theta_k + b \sin\left(\frac{2\pi k}{N}\right), \quad k = 1, 2, \dots, N, \\ 0 &< \theta_k < 2\pi, \end{aligned} \quad (10)$$

and the unit outward normal vector  $\mathbf{n} = (n_x, n_y) = (-\cos\theta, -\sin\theta)$  for the inner circular boundaries, we have

$$\frac{\partial \varphi}{\partial n} = b \cos\left(\frac{2\pi k}{N}\right) \sin \theta_k - b \sin\left(\frac{2\pi k}{N}\right) \cos \theta_k \quad \text{on } B_k, \quad (11)$$

where  $B_k$  ( $k = 1, 2, \dots, N$ ) is the  $k$ th boundary of the inner hole,  $\theta_k$  is the polar angle with respect to the origin of the  $k$ th hole. For the outer boundary, the traction-free condition is specified. Thus, the problem of torsion is reduced to find the warping function  $\varphi$  which satisfies Laplace equation of Eq. (6) and the Neumann boundary conditions of Eq. (11) for the inner boundary and zero traction on the outer boundary.

### 3 Method of solution

#### 3.1 The dual boundary integral equations and null-field integral equations

We apply the Fourier series expansions to approximate the potential  $u$  and its normal derivative on the boundary

$$\begin{aligned} u(s_k) &= a_0^k + \sum_{n=1}^{\infty} (a_n^k \cos n\theta_k + b_n^k \sin n\theta_k), \\ s_k &\in B_k, \quad k = 1, 2, \dots, N, \end{aligned} \quad (12)$$

$$\begin{aligned} t(s_k) &= p_0^k + \sum_{n=1}^{\infty} (p_n^k \cos n\theta_k + q_n^k \sin n\theta_k), \\ s_k &\in B_k, \quad k = 1, 2, \dots, N, \end{aligned} \quad (13)$$

where  $t(s_k) = \partial u(s_k) / \partial \mathbf{n}_s$ ,  $a_n^k$ ,  $b_n^k$ ,  $p_n^k$  and  $q_n^k$  ( $n = 0, 1, 2, \dots$ ) are the Fourier coefficients and  $\theta_k$  is the polar angle. The integral equation for the domain point can

be derived from the third Green's identity [Chen, J. T.; Hong, H. -K. (1999)], we have

$$\begin{aligned} 2\pi u(x) &= \int_B T(s, x) u(s) dB(s) - \int_B U(s, x) t(s) dB(s), \\ x &\in D, \end{aligned} \quad (14)$$

$$\begin{aligned} 2\pi \frac{\partial u(x)}{\partial \mathbf{n}_x} &= \int_B M(s, x) u(s) dB(s) - \int_B L(s, x) t(s) dB(s), \\ x &\in D, \end{aligned} \quad (15)$$

where  $s$  and  $x$  are the source and field points, respectively,  $D$  is the domain of interest,  $\mathbf{n}_s$  and  $\mathbf{n}_x$  denote the outward normal vectors at the source point  $s$  and field point  $x$ , respectively, and the kernel function  $U(s, x) = \ln r$ , ( $r \equiv |x - s|$ ), is the fundamental solution which satisfies

$$\nabla^2 U(s, x) = 2\pi \delta(x - s), \quad (16)$$

in which  $\delta(x - s)$  denotes the Dirac-delta function. The other kernel functions,  $T(s, x)$ ,  $L(s, x)$  and  $M(s, x)$ , are defined by

$$\begin{aligned} T(s, x) &\equiv \frac{\partial U(s, x)}{\partial \mathbf{n}_s}, \quad L(s, x) \equiv \frac{\partial U(s, x)}{\partial \mathbf{n}_x}, \\ M(s, x) &\equiv \frac{\partial^2 U(s, x)}{\partial \mathbf{n}_s \partial \mathbf{n}_x}, \end{aligned} \quad (17)$$

By collocating  $x$  outside the domain ( $x \in D^c$ ), we obtain the dual null-field integral equations as shown below

$$\begin{aligned} 0 &= \int_B T(s, x) u(s) dB(s) - \int_B U(s, x) t(s) dB(s), \\ x &\in D^c, \end{aligned} \quad (18)$$

$$\begin{aligned} 0 &= \int_B M(s, x) u(s) dB(s) - \int_B L(s, x) t(s) dB(s), \\ x &\in D^c, \end{aligned} \quad (19)$$

where  $D^c$  is the complementary domain. Based on the separable property, the kernel function  $U(s, x)$  can be expanded into degenerate form by separating the source points and field points in the polar coordinate [Chen J. T.; Chiu Y. P. (2002)]:

$$U(s, x) = \begin{cases} U^i(R, \theta; \rho, \phi) = \ln R \\ \quad - \sum_{m=1}^{\infty} \frac{1}{m} \left(\frac{\rho}{R}\right)^m \cos m(\theta - \phi), \quad R \geq \rho \\ U^e(R, \theta; \rho, \phi) = \ln \rho \\ \quad - \sum_{m=1}^{\infty} \frac{1}{m} \left(\frac{R}{\rho}\right)^m \cos m(\theta - \phi), \quad \rho > R \end{cases} \quad (20)$$

where the superscripts “*i*” and “*e*” denote the interior ( $R > \rho$ ) and exterior ( $\rho > R$ ) cases, respectively. In Eq. (20), the origin of the observer system for the degenerate kernel is (0,0) for simplicity. It is noted that degenerate kernel for the fundamental solution is equivalent to the addition theorem which was similarly used by Bird and Steele [Bird M. D.; Steele C. R. (1992)]. Figure 2 shows the graph of separate expressions of fundamental solutions where source point  $s$  located at  $R = 10.0, \theta = \pi/3$ .

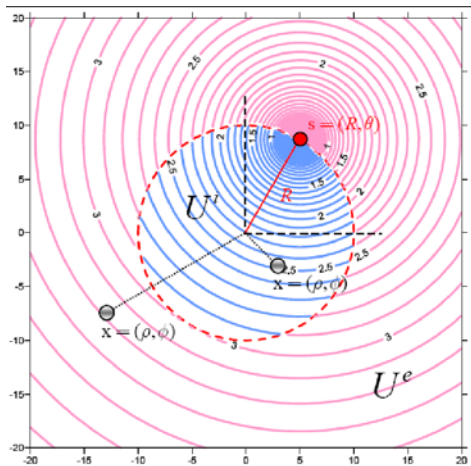


**Figure 2** : Graph of the separate form of fundamental solution ( $s = (10, \pi/3)$ )

By setting the origin at  $o$  for the observer system, a circle with radius  $R$  from the origin  $o$  to the source point  $s$  is plotted. If the field point  $x$  is situated inside the circular region, the degenerate kernel belongs to the interior case  $U^i$ ; otherwise, it is the exterior case. After taking the normal derivative  $\frac{\partial}{\partial R}$  with respect to Eq. (20), the  $T(s,x)$  kernel can be derived as

$$T(s,x) = \begin{cases} T^i(R,\theta;\rho,\phi) = \frac{1}{R} + \sum_{m=1}^{\infty} \left(\frac{\rho^m}{R^{m+1}}\right) \cos m(\theta - \phi), & R > \rho \\ T^e(R,\theta;\rho,\phi) = - \sum_{m=1}^{\infty} \left(\frac{R^{m-1}}{\rho^m}\right) \cos m(\theta - \phi), & \rho > R \end{cases}, \quad (21)$$

and the higher-order kernel functions,  $L(s,x)$  and  $M(s,x)$ ,

are shown below

$$L(s,x) = \begin{cases} L^i(R,\theta;\rho,\phi) = - \sum_{m=1}^{\infty} \left(\frac{\rho^{m-1}}{R^m}\right) \cos m(\theta - \phi), & R > \rho \\ L^e(R,\theta;\rho,\phi) = \frac{1}{\rho} + \sum_{m=1}^{\infty} \left(\frac{R^m}{\rho^{m+1}}\right) \cos m(\theta - \phi), & \rho > R \end{cases}, \quad (22)$$

$$M(s,x) = \begin{cases} M^i(R,\theta;\rho,\phi) = \sum_{m=1}^{\infty} \left(\frac{m\rho^{m-1}}{R^{m+1}}\right) \cos m(\theta - \phi), & R \geq \rho \\ M^e(R,\theta;\rho,\phi) = \sum_{m=1}^{\infty} \left(\frac{mR^{m-1}}{\rho^{m+1}}\right) \cos m(\theta - \phi), & \rho > R \end{cases}. \quad (23)$$

Since the potential resulted from  $T(s,x)$  and  $L(s,x)$  kernels are discontinuous across the boundary, the potentials of  $T(s,x)$  for  $R \rightarrow \rho^+$  and  $R \rightarrow \rho^-$  are different. This is the reason why  $R = \rho$  is not included in expressions of degenerate kernels for  $T(s,x)$  and  $L(s,x)$  in Eqs. (21) and (22).

### 3.2 Adaptive observer system

After moving the point of Eq. (18) to the boundary, the boundary integrals through all the circular contours are required. Since the boundary integral equations are frame indifferent, *i.e.* objectivity rule, the observer system is adaptively to locate the origin at the center of circle in the boundary integral. Adaptive observer system is chosen to fully employ the property of degenerate kernels. Figures 3 and 4 show the boundary integration for the circular boundaries in the adaptive observer system.

It is noted that the origin of the observer system is located on the center of the corresponding circle under integration to entirely utilize the geometry of circular boundary for the expansion of degenerate kernels and boundary densities. The dummy variable in the circular integration is angle ( $\theta$ ) instead of radial coordinate ( $R$ ).

### 3.3 Linear algebraic system

By moving the null-field point  $x_k$  to the  $k$ th circular boundary in the sense of limit for Eq. (18) in Fig. 3,

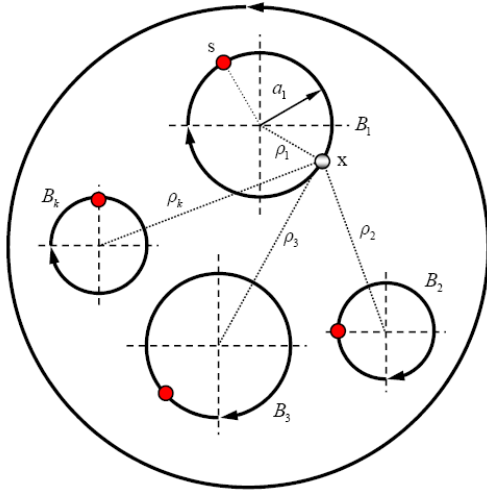


**Figure 3** : Sketch of the null-field integral equation in conjunction with the adaptive observer system

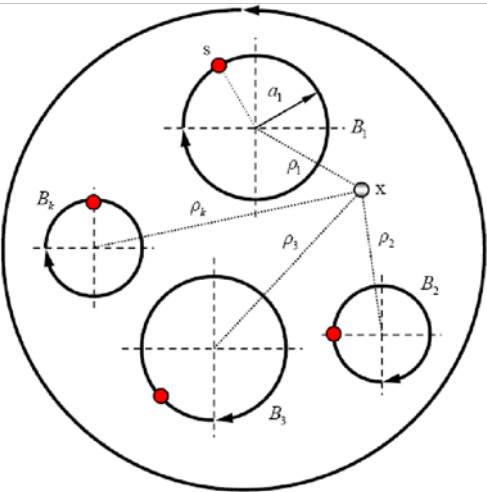


**Figure 4** : Sketch of the boundary integral equation for domain point inconjunction with the adaptive observer system

we have

$$0 = \sum_{k=1}^{N_C} \int_{B_k} T(s_k, x_j) u(s_k) dB_k(s) - \sum_{k=1}^{N_C} \int_{B_k} U(s_k, x_j) t(s_k) dB_k(s), \quad x \in D^c, \quad (24)$$

where  $N_C$  is the number of circles including the outer boundary and the inner circular holes. In the real computation, we select the collocation point on the boundary.

If the domain is unbounded, the outer boundary  $B_0$  is a null set and  $N_C = N$ . It is noted that the integration path is counterclockwise for the outer circle. Otherwise, it is clockwise. For the  $B_k$  integral of the circular boundary, the kernels of  $U(s, x)$  and  $T(s, x)$  are respectively expressed in terms of degenerate kernels of Eqs. (20) and (21), and  $u(s)$  and  $t(s)$  are substituted by using the Fourier series of Eqs. (12) and (13), respectively. In the  $B_k$  integral, we set the origin of the observer system to collocate at the center  $c_k$  to fully utilize the degenerate kernels and Fourier series. By collocating the null-field point on the boundary, a linear algebraic system is obtained

$$[\mathbf{U}] \{\mathbf{t}\} = [\mathbf{T}] \{\mathbf{u}\}, \quad (25)$$

where  $[\mathbf{U}]$  and  $[\mathbf{T}]$  are the influence matrices with a dimension of  $N_C(2M+1)$  by  $N_C(2M+1)$ ,  $\{\mathbf{u}\}$  and  $\{\mathbf{t}\}$  denote the column vectors of Fourier coefficients with a dimension of  $N_C(2M+1)$  by 1 in which  $[\mathbf{U}]$ ,  $[\mathbf{T}]$ ,  $\{\mathbf{u}\}$  and  $\{\mathbf{t}\}$  can be defined as follows:

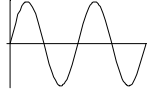
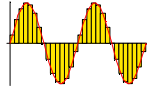
$$[\mathbf{U}] = \begin{bmatrix} \mathbf{U}_{00} & \mathbf{U}_{01} & \cdots & \mathbf{U}_{0N} \\ \mathbf{U}_{10} & \mathbf{U}_{11} & \cdots & \mathbf{U}_{1N} \\ \vdots & \vdots & \ddots & \vdots \\ \mathbf{U}_{N0} & \mathbf{U}_{N1} & \cdots & \mathbf{U}_{NN} \end{bmatrix}, \quad (26)$$

$$[\mathbf{T}] = \begin{bmatrix} \mathbf{T}_{00} & \mathbf{T}_{01} & \cdots & \mathbf{T}_{0N} \\ \mathbf{T}_{10} & \mathbf{T}_{11} & \cdots & \mathbf{T}_{1N} \\ \vdots & \vdots & \ddots & \vdots \\ \mathbf{T}_{N0} & \mathbf{T}_{N1} & \cdots & \mathbf{T}_{NN} \end{bmatrix},$$

$$\{\mathbf{u}\} = \begin{bmatrix} \mathbf{u}_0 \\ \mathbf{u}_1 \\ \mathbf{u}_2 \\ \vdots \\ \mathbf{u}_N \end{bmatrix}, \quad \{\mathbf{t}\} = \begin{bmatrix} \mathbf{t}_0 \\ \mathbf{t}_1 \\ \mathbf{t}_2 \\ \vdots \\ \mathbf{t}_N \end{bmatrix}, \quad (27)$$

where the vectors  $\{\mathbf{u}_k\}$  and  $\{\mathbf{t}_k\}$  are in the form of  $\{a_0^k \ a_1^k \ b_1^k \ \cdots \ a_M^k \ b_M^k\}^T$  and  $\{p_0^k \ p_1^k \ q_1^k \ \cdots \ p_M^k \ q_M^k\}^T$ , respectively; the first subscript “ $j$ ” ( $j = 0, 1, 2, \dots, N$ ) in  $[\mathbf{U}_{jk}]$  and  $[\mathbf{T}_{jk}]$  denotes the index of the  $j$ th circle where the collocation point is located and the second subscript “ $k$ ” ( $k = 0, 1, 2, \dots, N$ ) denotes the index of the  $k$ th circle where boundary data  $\{\mathbf{u}_k\}$  or  $\{\mathbf{t}_k\}$  are specified,  $N$  is the number of circular holes in the domain and

**Table 1** : Comparisons of the present method and conventional BEM

	Boundary density discretization	Auxiliary system	Formulation	Observer system	Singularity
Present method	Fourier series 	Degenerate kernel	Null-field integral equation	Adaptive observer system	No principal value
Conventional BEM	Constant element 	Fundamental solution	Boundary integral equation	Fixed observer system	Principal value (CPV, RPV and HPV)

**Table 2** : Torsional rigidity of circular cylinder with an eccentric hole ( $a/R = 1/3$ )

$\frac{b}{R-a}$	$2G/\mu\pi R^4$			
	Present method	Exact solution [Muskhelishvili NI (1953)]	BIE formulation [Caulk DA (1983)]	
			20 divisions	40 divisions
0.20	0.97872	0.97872	0.97873	0.97872
0.40	0.95137	0.95137	0.95140	0.95137
0.60	0.90312	0.90312	0.90328	0.90316
0.80	0.82473	0.82473	0.82574	0.82497
0.90	0.76168	0.76168	0.76583	0.76252
0.92	0.74455	0.74454	0.75057	0.74569
0.94	0.72451	0.72446	0.73367	0.72605
0.96	0.69991	0.69968	0.71473	0.70178
0.98	0.66705	0.66555	0.69321	0.66732

**Table 3** : Torsional rigidity of a circular cylinder with a ring of  $N$  holes ( $a/R = 1/4, b/R = 1/2$ )

Number of holes	$2G/\mu\pi R^4$		
	Present method	BIE formulation [Caulk DA (1983)]	First-order solution [Caulk DA (1983)]
2	0.8657	0.8657	0.8661
3	0.8214	0.8214	0.8224
4	0.7893	0.7893	0.7934

$M$  indicates the truncated terms of Fourier series. The influence coefficient matrix of the linear algebraic system is partitioned into blocks, and each off-diagonal block corresponds to the influence matrices between two different circular holes. The diagonal blocks are the influence matrices due to itself in each individual

hole. After uniformly collocating the point along the  $k$ th circular boundary, the submatrix can be written as

$$[\mathbf{U}_{jk}] = \begin{bmatrix} U_{jk}^{0c}(\phi_1) & U_{jk}^{1c}(\phi_1) & U_{jk}^{1s}(\phi_1) \\ U_{jk}^{0c}(\phi_2) & U_{jk}^{1c}(\phi_2) & U_{jk}^{1s}(\phi_2) \\ U_{jk}^{0c}(\phi_3) & U_{jk}^{1c}(\phi_3) & U_{jk}^{1s}(\phi_3) \\ \vdots & \vdots & \vdots \\ U_{jk}^{0c}(\phi_{2M}) & U_{jk}^{1c}(\phi_{2M}) & U_{jk}^{1s}(\phi_{2M}) \\ U_{jk}^{0c}(\phi_{2M+1}) & U_{jk}^{1c}(\phi_{2M+1}) & U_{jk}^{1s}(\phi_{2M+1}) \\ \cdots & U_{jk}^{Mc}(\phi_1) & U_{jk}^{Ms}(\phi_1) \\ \cdots & U_{jk}^{Mc}(\phi_2) & U_{jk}^{Ms}(\phi_2) \\ \cdots & U_{jk}^{Mc}(\phi_3) & U_{jk}^{Ms}(\phi_3) \\ \cdots & \vdots & \vdots \\ \cdots & U_{jk}^{Mc}(\phi_{2M}) & U_{jk}^{Ms}(\phi_{2M}) \\ \cdots & U_{jk}^{Mc}(\phi_{2M+1}) & U_{jk}^{Ms}(\phi_{2M+1}) \end{bmatrix}, \quad (28)$$

$$[\mathbf{T}_{jk}] = \begin{bmatrix} T_{jk}^{0c}(\phi_1) & T_{jk}^{1c}(\phi_1) & T_{jk}^{1s}(\phi_1) \\ T_{jk}^{0c}(\phi_2) & T_{jk}^{1c}(\phi_2) & T_{jk}^{1s}(\phi_2) \\ T_{jk}^{0c}(\phi_3) & T_{jk}^{1c}(\phi_3) & T_{jk}^{1s}(\phi_3) \\ \vdots & \vdots & \vdots \\ T_{jk}^{0c}(\phi_{2M}) & T_{jk}^{1c}(\phi_{2M}) & T_{jk}^{1s}(\phi_{2M}) \\ T_{jk}^{0c}(\phi_{2M+1}) & T_{jk}^{1c}(\phi_{2M+1}) & T_{jk}^{1s}(\phi_{2M+1}) \\ \cdots & T_{jk}^{Mc}(\phi_1) & T_{jk}^{Ms}(\phi_1) \\ \cdots & T_{jk}^{Mc}(\phi_2) & T_{jk}^{Ms}(\phi_2) \\ \cdots & T_{jk}^{Mc}(\phi_3) & T_{jk}^{Ms}(\phi_3) \\ \cdots & \vdots & \vdots \\ \cdots & T_{jk}^{Mc}(\phi_{2M}) & T_{jk}^{Ms}(\phi_{2M}) \\ \cdots & T_{jk}^{Mc}(\phi_{2M+1}) & T_{jk}^{Ms}(\phi_{2M+1}) \end{bmatrix}. \quad (29)$$

Although the matrices in Eqs. (28) and (29) are not sparse, they are diagonally dominant. It is found that the influence coefficient for the higher-order harmonics is smaller. It is noted that the superscript “0s” in Eqs. (28) and (29) disappears since  $\sin\theta = 0$ . The element of  $[\mathbf{U}_{jk}]$  and  $[\mathbf{T}_{jk}]$  are defined respectively as

$$U_{jk}^{nc}(\phi_m) = \int_{B_k} U(s_k, x_m) \cos(n\theta_k) R_k d\theta_k, \\ n = 0, 1, 2, \dots, M, \quad m = 1, 2, \dots, 2M+1, \quad (30)$$

$$U_{jk}^{ns}(\phi_m) = \int_{B_k} U(s_k, x_m) \sin(n\theta_k) R_k d\theta_k, \\ n = 1, 2, \dots, M, \quad m = 1, 2, \dots, 2M+1, \quad (31)$$

$$T_{jk}^{ns}(\phi_m) = \int_{B_k} T(s_k, x_m) \cos(n\theta_k) R_k d\theta_k, \\ n = 0, 1, 2, \dots, M, \quad m = 1, 2, \dots, 2M+1, \quad (32)$$

$$T_{jk}^{ns}(\phi_m) = \int_{B_k} T(s_k, x_m) \sin(n\theta_k) R_k d\theta_k, \\ n = 1, 2, \dots, M, \quad m = 1, 2, \dots, 2M+1, \quad (33)$$

where  $k$  is no sum and  $\phi_m$  is the polar angle of the collocating points  $x_m$  along the boundary. The explicit forms of all the boundary integrals for  $U, T, L$  and  $M$  kernels are listed in the Appendix. Besides, the limiting case across the boundary ( $R^- < \rho < R^+$ ) is also addressed. The continuous and jump behavior across the boundary is also described. By rearranging the known and unknown sets, the unknown Fourier coefficients are determined. Equation (18) can be calculated by employing the relations of trigonometric function and the orthogonal property in the real computation. Only the finite  $M$  terms are used in the summation of Eqs. (12) and (13). After obtaining the unknown Fourier coefficients, the origin of observer system is set to  $c_k$  in the  $B_k$  integration as shown in Fig. 4 to obtain the interior potential by employing Eq. (14). The differences between the present formulation and the conventional BEM are listed in Table 1.

#### 4 Illustrative examples and discussions

In this section, we deal with the torsion problems which have been solved by Caulk in 1983 [Caulk D. A. (1983)]. The contours of the axial displacement are plotted in three cases. The torsional rigidity of each example is calculated after determining the unknown Fourier coefficients.

##### Case 1: A circular bar with an eccentric hole

A circular bar of radius  $R$  with an eccentric circular holes removed is under torque  $T$  at the end. The torsional rigidity  $G$  of cross section can be expressed by

$$\frac{G}{\mu} = \int_D r^2 dD - \sum_{k=1}^N \int_{B_k} \phi \frac{\partial \phi}{\partial n} dB_k, \quad (34)$$

The results of torsional rigidity for each case are shown in Table 2. The exact solution derived by Muskhelishvili is listed in Table 2 for comparison.

Our solution is better than that of Caulk obtained by BIE when the hole is closely spaced.

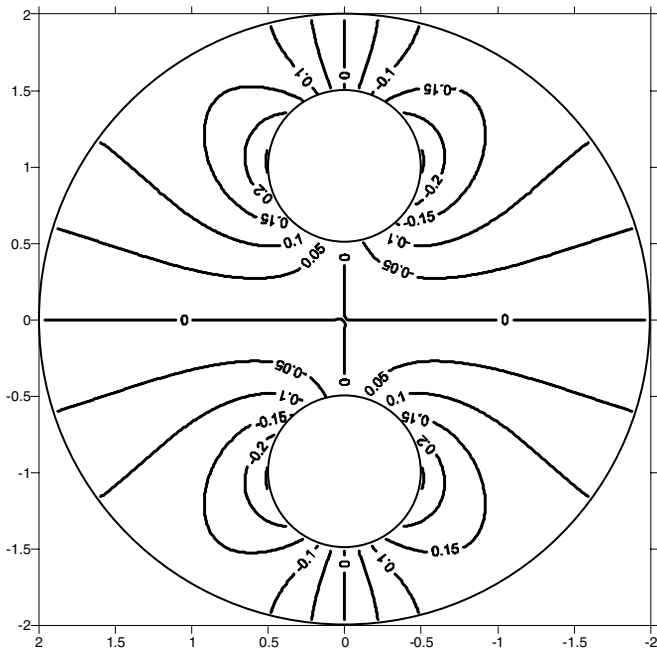


Figure 5 : Axial displacement for the circular bar weakened by two holes

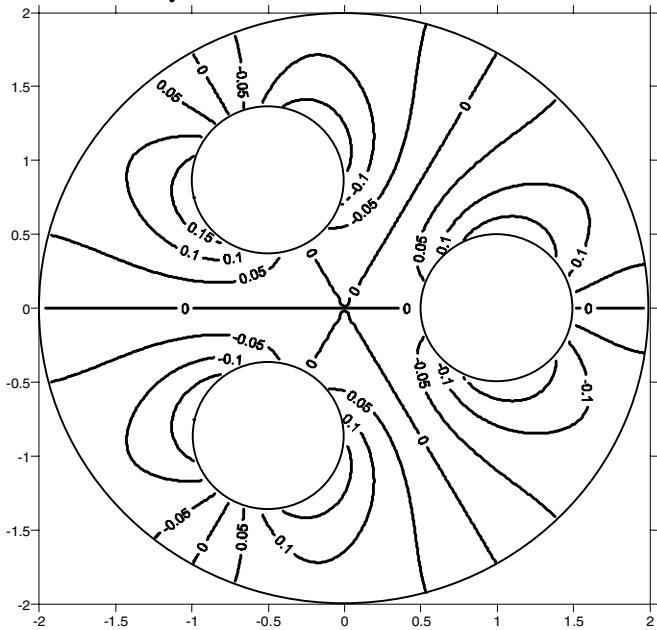


Figure 7 : Axial displacement for the circular bar weakened by three holes

Case 2: A circular bar with two circular holes

A circular bar of radius  $b$  with two equal circular holes removed is under torque  $T$  at the end. The boundary curve of  $k$ th inner cavity is described by using the parametric form of  $(x_k, y_k)$  in Eqs. (9) and (10). What is brought out is the problem subject to zero traction on the outer bound-

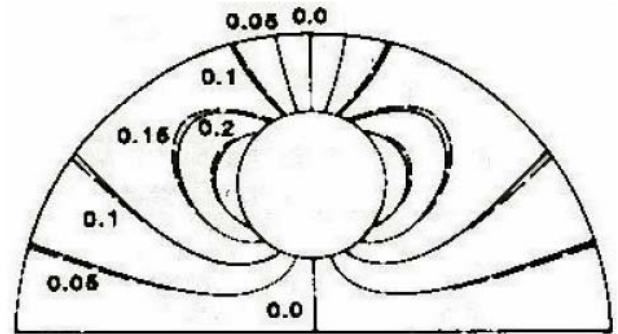


Figure 6 : Caulk's data (Solid lines indicate results from the first-order solution and dashed lines from the numerical solution of the exact boundary integral equation) [Caulk D. A. (1983)]

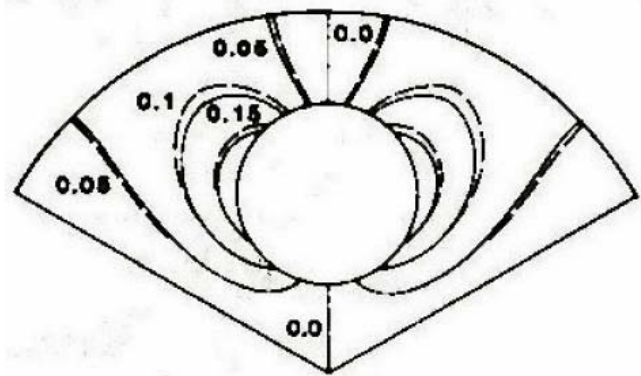
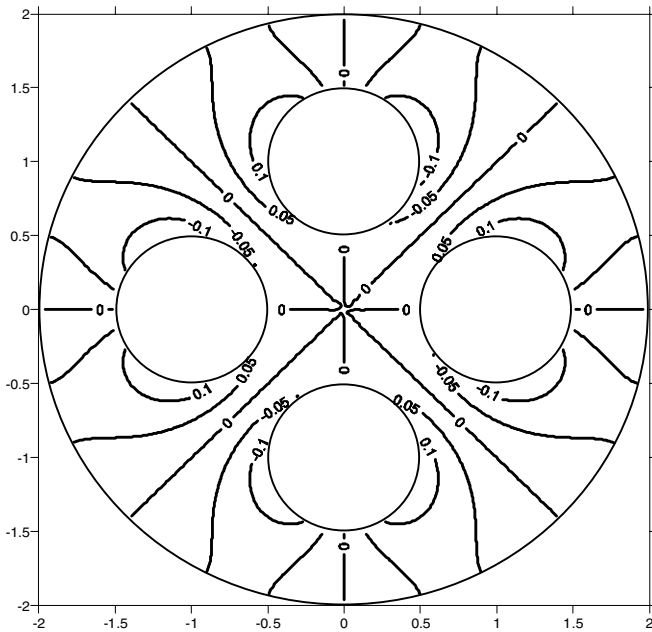


Figure 8 : Caulk's data (Solid lines indicate results from the first-order solution and dashed lines from the numerical solution of the exact boundary integral equation) [Caulk D. A. (1983)]

ary and Neumann boundary condition defined in Eq. (11) on all the inner circles. Figures 5 and 6 show the results using the present method and those from the first-order approximation solution and the exact boundary integral equation derived by Caulk [Caulk D. A. (1983)]. Twenty-one collocating points are selected on all the cir-





**Figure 9** : Axial displacement for the circular bar weakened by four holes

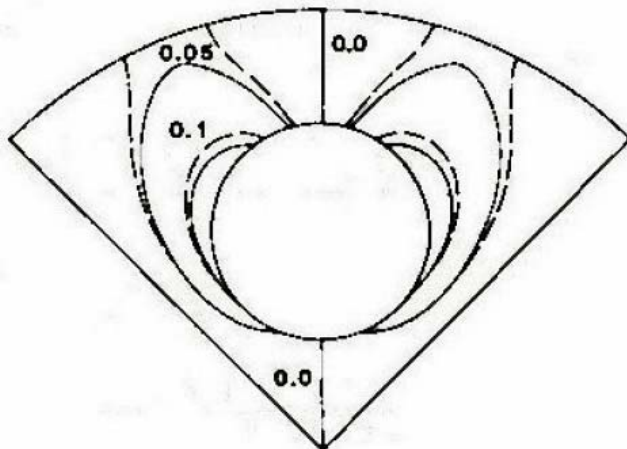


**Figure 10** : Caulk’s data (Solid lines indicate results from the first-order solution and dashed lines from the numerical solution of the exact boundary integral equation) [Caulk D. A. (1983)]

cular boundaries in the numerical implementation. After being compared with the results of Figure 6, the numerical results are consistent with those of the boundary integral equation.

*Case 3: A circular bar with three circular holes*

Unlike Case 2, a circular bar weakened by three circular

holes of equal radii is regarded as the third example. In a similar way, the contour plot of the axial displacement is shown in Figure 7. Good agreement is made after comparing with the Caulk’s data in Figure 8.

*Case 4: A circular bar with four circular holes*

The fourth problem is a circular bar weakened by four equal circular holes under torque. In Figure 9, our result of axial displacement agrees well with the values in the dashed line of Figure 10 which are solved by using the boundary integral equation. Results obtained by using the present method for Case 2, Case 3 and Case 4 are listed in Table 3. After comparison, our results agree well with Caulk’s data obtained by BIE formulation.

*Case 5: Ling’s examples [Ling C. B. (1947)]*

Table 4 shows a comparison of the torsional rigidities of three cases with different geometries of circular holes computed from the present method, BIE formulation [Caulk D. A. (1983)] and first-order approach [Caulk D. A. (1983)].

We have not only calculated the torsional rigidity but also tested the rate of convergence of Fourier terms of the case with seven cavities as shown in Fig 11. Test of Parseval’s sum for boundary densities was also implemented to ensure the convergence.

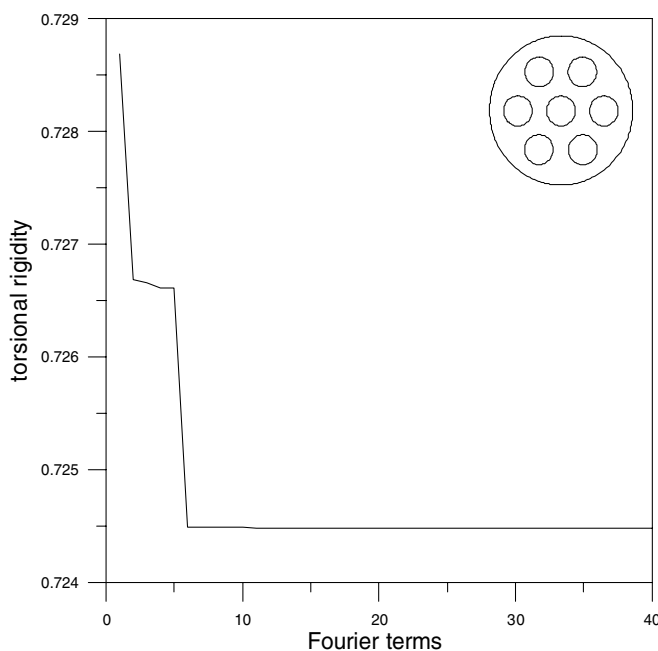
The present solutions are an improvement over Ling’s results in every case. The large difference in the second example in Table 4 may ascribe to Ling’s lengthy calculation in error as pointed out by Caulk [Caulk D. A. (1983)].

**5 Conclusions**

The torsion problems of circular shaft weakened by several holes have been successfully solved by using the present formulation. Our solutions match well with the exact solution and other solutions by using the boundary integral equation for the three Caulk’s cases. There are only 41 collocation points uniformly distributed on each boundary for more accurate results of torsional rigidity with error less than 1 % after comparing with the known exact solution. Regardless of the number of circles, the proposed method has great accuracy and generality. Through the solution for several problems, our method was successfully applied to cases of multiple holes. Furthermore, our method presented here can be used to problems which satisfy the Laplace operator.

**Table 4** : Torsional rigidity of Ling's [Ling C. B. (1947) ] examples

Case	$2G / \mu\pi R^4$		
	Present method	BIE formulation [Caulk DA (1983)]	Ling's results [Ling CB (1947)]
$N = 2, c/R = 0$ $a/R = 2/7, b/R = 3/7$	0.8712	0.8713	0.8809
$N = 2, c/R = 1/5$ $a/R = 1/5, b/R = 3/5$	0.8732	0.8732	0.8093
$N = 6, c/R = 1/5$ $a/R = 1/5, b/R = 3/5$	0.7245	0.7261	0.7305

**Figure 11** : Torsion rigidity versus the number of Fourier terms

**Acknowledgement:** Financial support from the National Science Council under Grant No. NSC91-2211-E-019-009 for Taiwan Ocean University is gratefully acknowledged.

## References

- Ang W. T.; Kang I.** (2000): "A complex variable boundary element method for elliptic partial differential equations in a multiply-connected region", *International Journal of Computer Mathematics*, **75**, 515-525.
- Bird M. D.; Steele C. R.** (1992): "A solution procedure for Laplace's equation on multiple connected circular domains", *ASME Journal of Applied Mechanics*, **59**, 398-

404.

**Bird M. D.; Steele C. R.** (1991): "Separated solution procedure for bending of circular plates with circular holes", *ASME Journal of Applied Mechanics*, **59**, 398-404.

**Caulk D. A.** (1983): "Analysis of elastic torsion in a bar with circular holes by a special boundary integral method", *ASME Journal of Applied Mechanics*, **50**, 101-108.

**Chen J. T.; Chiu Y. P.** (2002): "On the pseudo-differential operators in the dual boundary integral equations using degenerate kernels and circulants", *Engineering Analysis with Boundary Elements*, **26**, 41-53.

**Chen J. T.; Hong H. K.** (1999): "Review of dual boundary element methods with emphasis on hypersingular integrals and divergent series", *ASME Applied Mechanics Reviews*, **52**, pp. 17-33.

**Chen T.; Weng I. S.** (2001): "Torsion of a circular compound bar with imperfect interface", *Journal of Applied Mechanics, ASME*, **68**, 955-958.

**Crouch S. L.; Mogilevskaya S .G.** (2003): "On the use of Somigliana's formula and Fourier series for elasticity problems with circular boundaries", *International Journal for Numerical Methods in Engineering*, **58**, 537-578.

**Jin B.** (2004): "A meshless method for the Laplace and biharmonic equations subjected to noisy boundary data", *CMES: Computer Modeling in Engineering & Sciences*, **6 No. 3**, 253-262.

**Ling C. B.** (1947): "Torsion of a circular tube with longitudinal circular holes", *Quarterly of Applied Mathematics*, **5**, 168-181.

**Mogilevskaya S. G.; Crouch S. L.** (2001): "A Galerkin boundary integral method for multiple circular elastic inclusions", *International Journal for Numerical Methods*

in *Engineering*, **52**, 1069-1106.

**Muskhelishvili N. I.** (1953): "Some basic problems of the mathematical theory of elasticity", *Noordhoff*, Groningen.

**Shams-Ahmadi M.; Chou S. I.** (1997): "Complex variable boundary element method for torsion of composite shafts", *International Journal for Numerical Methods in Engineering*, **40**, 1165-1179.

**Sladek V.; Sladek J.; Tanaka M.** (2005): "Local integral equations and two meshless polynomial interpolations with application to potential problems in non-homogeneous media" *CMES: Computer Modeling in Engineering & Sciences*, **7 No. 1**, 69-84.

**Timoshenko S. P.; Goodier J. N.** (1970): "Theory of Elasticity", *McGraw-Hill*, New York.

**Wordelman C. J.; Aluru N. R.; Ravaoli U.** (2000): "A meshless method for the numerical solution of the 2- and 3-D semiconductor Poisson equation", *CMES: Computer Modeling in Engineering & Sciences*, **1 No. 1**, 121-126.

#### **Appendix A: Appendix**

*Analytical evaluation of the integrals and their limits.*

The degenerate kernels are described in Eqs. (20), (21), (22) and (23), and orthogonal process is shown below:

	$U(s,x)$ and $\int_B U(s,x)t(s)dB(s)$
Orthogonal process	$\begin{cases} \int_0^{2\pi} U^i \cos(n\theta)Rd\theta = \pi \frac{1}{n} \frac{\rho^n}{R^{n-1}} \cos(n\phi), R \geq \rho \\ \int_0^{2\pi} U^i \sin(n\theta)Rd\theta = \pi \frac{1}{n} \frac{\rho^n}{R^{n-1}} \sin(n\phi), R \geq \rho \\ \int_0^{2\pi} U^e \cos(n\theta)Rd\theta = \pi \frac{1}{n} \frac{R^{n+1}}{\rho^n} \cos(n\phi), R < \rho \\ \int_0^{2\pi} U^e \sin(n\theta)Rd\theta = \pi \frac{1}{n} \frac{R^{n+1}}{\rho^n} \sin(n\phi), R < \rho \end{cases}$
Limit $\rho \rightarrow R$	$\begin{cases} \pi \frac{1}{n} \frac{\rho^n}{R^{n-1}} \cos(n\phi) = \pi \frac{1}{n} R \cos(n\phi), R \geq \rho \\ \pi \frac{1}{n} \frac{\rho^n}{R^{n-1}} \sin(n\phi) = \pi \frac{1}{n} R \sin(n\phi), R \geq \rho \\ \pi \frac{1}{n} \frac{R^{n+1}}{\rho^n} \cos(n\phi) = \pi \frac{1}{n} R \cos(n\phi), R < \rho \\ \pi \frac{1}{n} \frac{R^{n+1}}{\rho^n} \sin(n\phi) = \pi \frac{1}{n} R \sin(n\phi), R < \rho \end{cases} \quad (\text{Continuous for } R^- < \rho < R^+)$
	$T(s,x)$ and $\int_B T(s,x)u(s)dB(s)$
Orthogonal process	$\begin{cases} \int_0^{2\pi} T^i \cos(n\theta)Rd\theta = \pi \left(\frac{\rho}{R}\right)^n \cos(n\phi), R > \rho \\ \int_0^{2\pi} T^i \sin(n\theta)Rd\theta = \pi \left(\frac{\rho}{R}\right)^n \sin(n\phi), R > \rho \\ \int_0^{2\pi} T^e \cos(n\theta)Rd\theta = -\pi \left(\frac{R}{\rho}\right)^n \cos(n\phi), R < \rho \\ \int_0^{2\pi} T^e \sin(n\theta)Rd\theta = -\pi \left(\frac{R}{\rho}\right)^n \sin(n\phi), R < \rho \end{cases}$
Limit $\rho \rightarrow R$	$\begin{cases} \pi \left(\frac{\rho}{R}\right)^n \cos(n\phi) = \pi \cos(n\phi), R > \rho \\ \pi \left(\frac{\rho}{R}\right)^n \sin(n\phi) = \pi \sin(n\phi), R > \rho \\ -\pi \left(\frac{R}{\rho}\right)^n \cos(n\phi) = -\pi \cos(n\phi), R < \rho \\ -\pi \left(\frac{R}{\rho}\right)^n \sin(n\phi) = -\pi \sin(n\phi), R < \rho \end{cases} \quad (\text{jump for } R^- < \rho < R^+)$
	$L(s,x)$ and $\int_B L(s,x)t(s)dB(s)$
Orthogonal process	$\begin{cases} \int_0^{2\pi} L^i \cos(n\theta)Rd\theta = -\pi \left(\frac{\rho}{R}\right)^{n-1} \cos(n\phi), R > \rho \\ \int_0^{2\pi} L^i \sin(n\theta)Rd\theta = -\pi \left(\frac{\rho}{R}\right)^{n-1} \sin(n\phi), R > \rho \\ \int_0^{2\pi} L^e \cos(n\theta)Rd\theta = \pi \left(\frac{R}{\rho}\right)^{n+1} \cos(n\phi), R < \rho \\ \int_0^{2\pi} L^e \sin(n\theta)Rd\theta = \pi \left(\frac{R}{\rho}\right)^{n+1} \sin(n\phi), R < \rho \end{cases}$
Limit $\rho \rightarrow R$	$\begin{cases} -\pi \left(\frac{\rho}{R}\right)^{n-1} \cos(n\phi) = -\pi \cos(n\phi), R > \rho \\ -\pi \left(\frac{\rho}{R}\right)^{n-1} \sin(n\phi) = -\pi \sin(n\phi), R > \rho \\ \pi \left(\frac{R}{\rho}\right)^{n+1} \cos(n\phi) = \pi \cos(n\phi), R < \rho \\ \pi \left(\frac{R}{\rho}\right)^{n+1} \sin(n\phi) = \pi \sin(n\phi), R < \rho \end{cases} \quad (\text{jump for } R^- < \rho < R^+)$
	$M(s,x)$ and $\int_B M(s,x)u(s)dB(s)$
Orthogonal process	$\begin{cases} \int_0^{2\pi} M^i \cos(n\theta)Rd\theta = n\pi \frac{\rho^{n-1}}{R^n} \cos(n\phi), R \geq \rho \\ \int_0^{2\pi} M^i \sin(n\theta)Rd\theta = n\pi \frac{\rho^{n-1}}{R^n} \sin(n\phi), R \geq \rho \\ \int_0^{2\pi} M^e \cos(n\theta)Rd\theta = n\pi \frac{R^n}{\rho^{n+1}} \cos(n\phi), R < \rho \\ \int_0^{2\pi} M^e \sin(n\theta)Rd\theta = n\pi \frac{R^n}{\rho^{n+1}} \sin(n\phi), R < \rho \end{cases}$
Limit $\rho \rightarrow R$	$\begin{cases} n\pi \frac{\rho^{n-1}}{R^n} \cos(n\phi) = n\pi \frac{1}{R} \cos(n\phi), R \geq \rho \\ n\pi \frac{\rho^{n-1}}{R^n} \sin(n\phi) = n\pi \frac{1}{R} \sin(n\phi), R \geq \rho \\ n\pi \frac{R^n}{\rho^{n+1}} \cos(n\phi) = n\pi \frac{1}{R} \cos(n\phi), R < \rho \\ n\pi \frac{R^n}{\rho^{n+1}} \sin(n\phi) = n\pi \frac{1}{R} \sin(n\phi), R < \rho \end{cases} \quad (\text{Continuous for } R^- < \rho < R^+)$